Electronic Structure, Isomerism, and Chemical Bonding in B7−and B7

ARTICLE *in* THE JOURNAL OF PHYSICAL CHEMISTRY A · MARCH 2004

Impact Factor: 2.69 · DOI: 10.1021/jp037341u

Electronic Structure, Isomerism, and Chemical Bonding in B_7^- and B_7

Anastassia N. Alexandrova and Alexander I. Boldyrev*

Department of Chemistry and Biochemistry, Utah State University, Logan, Utah 84322-0300

Hua-Jin Zhai and Lai-Sheng Wang†

Department of Physics, Washington State University, 2710 University Drive, Richland, Washington 99352 and W.R. Wiley Environmental Molecular Sciences Laboratory, Pacific Northwest National Laboratory, MS K8-88, P.O. Box 999, Richland, Washington 99352

Received: November 3, 2003; In Final Form: February 9, 2004

The electronic structure and chemical bonding of B_7^- and B_7 have been investigated using photoelectron spectroscopy and ab initio calculations. Complicated, but well-resolved, photoelectron spectra were obtained for B_7^- at several photon energies and were shown distinctly to contain contributions from different B_7^- isomers. The structures of the global minima and low-lying isomers were identified using extensive ab initio calculations. Two almost degenerate pyramidal structures I (C_{6v}, $^3A_1$) and II (C_{2v}, $^1A_1$) were the most stable for B_7^-. The triplet structure-I is slightly more stable than the singlet structure at our highest level of theory [RCCSD(T)/6-311+G(2df)] by 0.7 kcal/mol only. The next lowest singlet structure V (C_{2v}, $^1A_1$) was perfectly planar and was 7.8 kcal/mol higher in energy at RCCSD(T)/6-311+G(2df) level. The observed photoelectron spectra can only be explained when contributions from all these three low-lying isomers were considered; the observed spectral features were in good agreement with the calculated detachment transitions from the three isomers. Analyses of the molecular orbitals and chemical bonding revealed evidence that the triplet pyramidal C_{6v} structure-I has a twofold (π and σ) aromaticity, the singlet pyramidal C_{2v} structure-II has σ-aromaticity and π-antiaromaticity, and the singlet planar C_{2v} structure V has a twofold (π and σ) antiaromaticity.

1. Introduction

Boron—the element with a seemingly simple electronic structure—has a rather complex range of chemistry that is substantially different from that of its neighbor in the periodic table, carbon.[1,2] Although boron chemistry is dominated by three-dimensional (3D) structural motifs, such as the well-known B_{12} icosahedron, B_6 octahedron, and B_{12} cuboctahedron, recent theoretical studies have uncovered a highly unusual two-dimensional (2D) world for pure boron clusters.[3−34] Experimentally, mass-spectrometry-based studies have been carried out on small boron clusters,[4,35−41] but there have been no experimental confirmations of the 2D structures predicted in the theoretical studies. In an effort to elucidate the structure and bonding of small boron clusters, we have reported in a series of recent articles joint experimental and theoretical studies of several boron cluster species, including B_3^- and B_4^-,[42] B_5^-,[43] B_6^-,[44] B_8^- and B_9^-,[45] B_{10}^- $-B_{15}^-$,[46] and their neutrals. We have confirmed the 2D or quasi-2D nature of all these clusters and have shown that both σ- and π-aromaticity and antiaromaticity are responsible for the unique planar shapes of these boron clusters.

However, B_7^- and B_7 have been missing in our previous studies.[42−46] The B_7^- anionic cluster was the easiest boron cluster to be observed with our laser vaporization supersonic cluster source. But its photoelectron spectra turned out to be exceedingly complicated and congested and have posted a considerable challenge for our joint experimental and theoretical interrogation. An extensive and exhaustive experimental investigation using a variety of targets and experimental conditions was carried out, eventually revealing the coexistence of isomers in the B_7^- beam. Concurrently, extensive theoretical searches have led to the successful identification of several structural isomers for B_7^-. These experimental and theoretical efforts are reported in this article.

We found that a hexagonal pyramidal triplet (C_{6v}, $^3A_1$) structure I and a similar singlet (C_{2v}, $^1A_1$) isomer II of B_7^- were virtually degenerate and may serve as the global minimum, with the triplet being just 0.7 kcal/mol lower in energy at our highest level of theory. More interestingly, a third isomer, a perfect planar singlet V (C_{2v}, $^1A_1$) higher in energy, contributed significantly to the observed photoelectron spectra. A detailed analysis was carried out on the chemical bonding of the three isomers. We will also present evidence for double aromaticity (σ and π) in the triplet structure I, a single σ-aromaticity and a single π-antiaromaticity in the singlet isomer II, and a double antiaromaticity in the planar isomer V. The current synergistic experimental and theoretical efforts have led to a thorough understanding of the electronic and structural properties and chemical bonding in B_7^- and B_7, which represent one of the most unusual cluster systems that we have ever encountered.

2. Experimental Methods

The experiment was carried out using a magnetic bottle time-of-flight photoelectron apparatus equipped with a laser vaporization supersonic cluster source.[47] Briefly, the B_7^- anions were produced by laser vaporization of a boron-containing disk target in the presence of a helium carrier gas. Various boron clusters were produced from the cluster source and were analyzed using

* Address correspondence to this author. E-mail: boldyrev@cc.usu.edu.
† E-mail: ls.wang@pnl.gov.

10.1021/jp037341u CCC: $27.50
Published on Web 03/20/2004

a time-of-flight mass spectrometer. The cluster species of interest (B_7^-) were mass-selected and decelerated before being photodetached. Three detachment photon energies were used in the current experiments: 355 nm (3.496 eV), 266 nm (4.661 eV), and 193 nm (6.424 eV). Photoelectron spectra were calibrated using the known spectrum of Rh^-, and the resolution of the apparatus was better than 30 meV for 1 eV electrons.

The B_7^- cluster was very easy to produce from our laser vaporization source. Without optimizing the source conditions, the B_7^- cluster would be the smallest boron cluster anions observed with any significant abundance, as also shown recently by Xu et al.[48] However, the photoelectron spectra of B_7^- exhibited complicated spectral patterns and high quality data were rather challenging to be obtained. To rule out possibilities of impurity contributions, various boron-containing targets were used to generate B_7^-. We initially used boron targets with the natural isotopes (19.8% ^{10}B and 80.2% ^{11}B), from which the B_7^- mass peaks span a range from 70 to 77 amu. At this low mass range, our mass spectrometer could resolve the different peaks to the baseline. The two abundant masses at 76 and 77 amu were selected for photodetechment. We did observe contaminations in the spectra of the 76 amu peak of B_7^- from $B_4O_2^-$ because one of its isotope peaks ($^{11}B_4O_2^-$) also has the same mass. However, the 77 amu peak ($^{11}B_7^-$) was much cleaner and free from the oxide contamination. We also used ^{10}B isotope-enriched (99.75%) targets, which gave much simplified mass spectra and allowed complete separation of $^{10}B_7^-$ (70 amu) from $^{10}B_4O_2^-$ (72 amu). Finally, in a separate experiment, we were able to produce B_7^- from a ^{10}B/Li mixed target. This target yielded B_7^- at different source conditions from the pure targets and allowed variations of relative ratios of different isomers, if any, in the mass-selected B_7^- beam. With these efforts, we were able to completely rule out any contaminations in the B_7^- photoelectron spectra and were able to observe distinct contributions from isomers to the observed spectra, as shown below in Section 4.

3. Theoretical Methods

Initially, an extensive search of the global minima structures of B_7 and B_7^- was performed, employing a hybrid method, which included a mixture of Hartree−Fock exchange with density functional exchange-correlation potentials (B3LYP).[49−51] Analytical gradients with the polarized split-valence basis sets (6-311+G*)[52−54] were used. For the lowest energy structures, geometries and energies were refined using the restricted coupled cluster method [RCCSD(T)][55−57] with the same basis set. Additional energy refining was done with more extended 6-311+G(2df) basis set. To test the validity of the one-electron approximation, single-point calculations were performed using the multiconfiguration self-consistent field method (CASSCF)[58,59] with eight active electrons and eight active molecular orbitals for all singlet and triplet low-lying species [CASSCF-(8,8)/6-311+G*].

For the four lowest isomers found for B_7^-, we calculated their theoretical photoelectron spectra. For the singlet isomers of B_7^-, only transitions into the final doublet states were calculated. For the triplet isomers of B_7^-, transitions into the doublet and quadruplet states were calculated. The vertical electron detachment energies (VDE) were initially calculated using the restricted (for singlet states) and unrestricted (for triplet states) outer-valence Green function (R(U)OVGF) method[60−64] with extended basis set (6-311+G(2df)). The selection of the renormalization procedure in the OVGF calculations was done as it is implemented in Gaussian-98.[65] We also calculated VDEs

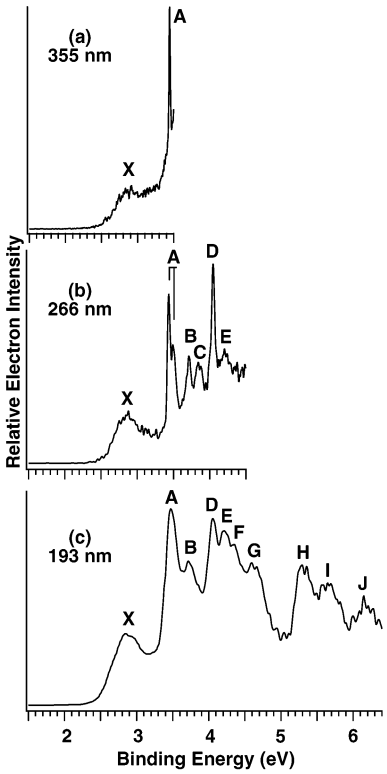

Figure 1. Photoelectron spectra of B_7^- at (a) 355 nm (3.496 eV), (b) 266 nm (4.661 eV), and (c) 193 nm (6.424 eV).

using the RCCSD(T)/6-311+G(2df) method. All low-energy transitions were also evaluated using time-dependent density functional methods[66,67] (TD-B3LYP and TD-BPW91) with the extended 6-311+G(2df) basis set. In this approach, the vertical electron detachment energies were calculated as a sum of the lowest transitions from the singlet (or triplet) anion into the final lowest doublet (or quartet) state of the neutral species (at the B3LYP or BPW91 level of theory) and the vertical excitation energies in the neutral species (at the TD-B3LYP or TD-BPW91 level of theory, respectively).

The chemical bonding in the clusters was characterized via molecular orbital analysis, which was done at the RHF/6-311+G* and UHF/6-311+G* levels of theory.

All B3LYP, CASSCF(8,8), TD-B3LYP, and TD-BPW91 calculations were performed using the Gaussian-03 program.[68] The R(U)OVGF calculations were performed using the Gaussian-98 program.[69] The RCCSD(T)/6-311+G* and RCCSD(T)/6-311+G(2df) calculations were performed using the Molpro-1999 program.[70] Molecular orbital pictures (RHF/6-311+G* and UHF/6-311+G*) were made using the MOLDEN 3.4 program.[71] Calculations were performed on a 63-nodes Birch-Retford Beowulf cluster computer built at Utah State University by K. A. Birch and B. P. Retford.

4. Experimental Results

Figure 1 shows the photoelectron spectra of B_7^- at three photon energies. All data shown were taken with the ^{10}B enriched target ($^{10}B_7^- = 70$ amu). Spectra taken with the natural isotope boron target for two masses 76 and 77 amu were used to rule out the $B_4O_2^-$ contaminations. With the ^{10}B enriched target, we were able to completely separate B_7^- (70 amu) and $B_4O_2^-$ (72 amu) in the mass spectrum. The oxide cluster was present with weaker abundance and its photoelectron spectra were cleanly obtained with well-resolved sharp features (unpublished). The fact that identical photoelectron spectra were

TABLE 1: Observed Adiabatic and Vertical Binding Energies (ADEs and VDEs) and Vibrational Frequencies from the Photoelectron Spectra of B_7^-

observed features	ADE (eV)[a]	VDE (eV)[a]	vibr. frequency (cm^{-1})[a]
X	2.55 (5)[b]	2.85 (5)	
A	3.44 (2)[b]	3.44 (2)	480 (40)
B		3.71 (4)	
C		3.84 (5)	
D		4.05 (3)	
E		4.21 (5)	
F		4.35 (5)	
G		4.60 (5)	
H		5.32 (5)	
I		5.64 (5)	
J		6.15 (5)	

[a] Numbers in parentheses represent the experimental uncertainties in the last digits. [b] The ADEs also define the adiabatic electron affinities of the corresponding neutral isomers of B_7. See text for details.

obtained for the different isotope peaks of B_7^- suggested that the complicated spectral features shown in Figure 1 were free from any contributions from contaminants in the B_7^- beam.

The 355-nm spectrum of B_7^- (Figure 1a) revealed a broad threshold feature (X) with a VDE of ~2.85 eV. A very sharp and intense feature (A) was also observed at 3.44 eV. At 266 nm (Figure 1b), the A band were observed to have a short vibrational progression with a spacing of 480 (40) cm^{-1}. Four more sharp features were identified at higher binding energies: B (3.71 eV), C (3.84 eV), D (4.05 eV), and E (4.21 eV). The 193-nm spectrum (Figure 1c) further revealed a few more well-defined features: F (4.35 eV), G (4.60 eV), H (5.32 eV), I (5.64 eV), and J (6.15 eV). Features D, E, F, and G appeared rather congested and spanned a narrow energy range of ~0.6 eV, which was followed by a gap of ~0.7 eV to the next feature H. Overall, 11 well-defined features were identified from the PES data; their vertical VDEs were evaluated from the peak maxima and are listed in Table 1. The adiabatic detachment energies (ADEs) of features X and A were also evaluated from the PES data. For feature A, the 0−0 vibrational transition defined an accurate ADE of 3.44 eV. For feature X, no vibrational structures were resolved, and the ADE was evaluated by drawing a straight line at the leading edge of the band and then adding a constant to the intersection with the binding energy axis to take into account the instrumental resolution. The ADEs of the X and A bands were also collected in Table 1, which also represent the electron affinities (EAs) of two isomers of neutral B_7, as will be shown below.

Figure 2 shows the experimental evidence for the coexistence of isomers in the B_7^- beam. Figure 2a displays the same data as Figure 1c, which was taken with the pure ^{10}B enriched target. Figure 2b presents the spectrum taken with a ^{10}B/Li mixed target, which gave pure boron clusters in addition to the B/Li mixed clusters but at different source conditions relative to a pure boron target. Surprisingly, the relative intensities of the spectral features are quite different in the two data sets: the intensities of features A, B, and G were significantly decreased in Figure 2b compared to the spectrum in Figure 2a. Since we were able to eliminate any possibilities for contamination, this observation indicated that feature A, B, and G came from a different isomer of B_7^-. Even though we had the ability to control the cluster temperatures to some degree with our cluster source,[72] we were not able to alter the populations of the two isomers of B_7^- significantly when pure boron targets were used in the laser vaporization. This was responsible for the fact that for a long time we were not able to interpret the B_7^- data. As will be shown below from our theoretical studies, the B_7^- spectra

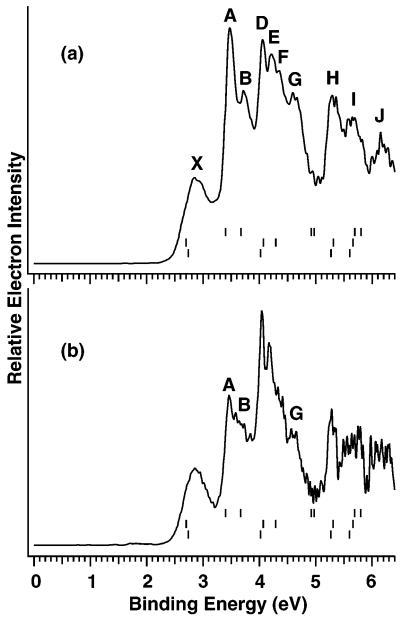

Figure 2. Photoelectron spectra of B_7^- at two different conditions. The B_7^- cluster beam was produced with (a) a ^{10}B enriched target and (b) a ^{10}B/Li mixed target, respectively. Note the intensity variation of features A, B, and G from a to b, indicating that these features were from a different isomer of B_7^-. The vertical bars were theoretical VDEs at the OVGF level of theory for isomers I, II, and V (from bottom row up), respectively (see text).

in fact had contributions from three isomers, whose calculated VDEs were plotted as vertical bars in Figure 2.

5. Theoretical Results

Our extensive search for the global minimum structure of the anionic B_7^- species at the B3LYP/6-311+G* level of theory revealed that there are two low energy structures I and II (Figure 3, Tables 2 and 3) with the pyramidal shape. The global minimum at this level of theory was structure I (C_{6v}, $^3A_1$) with the electronic configuration ($1a_1^2 1e_1^4 1e_2^4 2a_1^2 3a_1^2 1b_1^2 2e_1^4 3e_1^2$). The deviation from planarity in structure I is not significant, and the planar saddle point structure III (D_{6h}, $^3A_{1g}$, Figure 3) is just 5.5 kcal/mol higher in energy. The second lowest energy structure II at this level of theory can be considered as derived from structure I with one degenerate HOMO occupied by two electrons, inducing a Jahn−Teller distortion. The resulting structure II (C_{2v}, $^1A_1$) with the ($1a_1^2 1b_2^2 1b_1^2 2a_1^2 1a_2^2 3a_1^2 2b_1^2$-$4a_1^2 2b_2^2 3b_1^2 3b_2^2$) electronic configuration was just 3.9 kcal/mol higher in energy than structure I. There are also two other planar low-lying local minimum structures IV (C_{2v}, $^3B_2$) and V (C_{2v}, $^1A_1$) with the configurations $1a_1^2 1b_2^2 2a_1^2 3a_1^2 2b_2^2 1b_1^2 3b_2^2 4a_1^2$-$5a_1^2 1a_2^2 4b_2^1 6a_1^1$ and $1a_1^2 1b_2^2 2a_1^2 3a_1^2 2b_2^2 3b_2^2 1b_1^2 4a_1^2 5a_1^2 1a_2^2$-$4b_2^2$, respectively (Figure 3, Table 4). They were 8.2 and 11.0 kcal/mol higher than structure I at the B3LYP/6-311+G* level. At the RCCSD(T)/6-311+G(2df) level of theory, they were 16.9 and 7.8 kcal/mol above the global minimum, respectively, that is, the singlet planar structure V is much more stable than the triplet planar structure IV.

The geometries of these lowest-lying isomers were then refined at the RCCSD(T)/6-311+G* and the final relative energies were estimated at the RCCSD(T)/6-311+G(2df)//RCCSD(T)/6-311+G* level of theory. At our highest level of theory, we found that the triplet structure I (C_{6v}, $^3A_1$) is lower in energy than the singlet structure II (C_{2v}, $^1A_1$) by just 0.7 kcal/mol. Thus, these two structures are almost degenerate. The single-point CASSCF(8,8)/6-311+G(2df) calculations showed

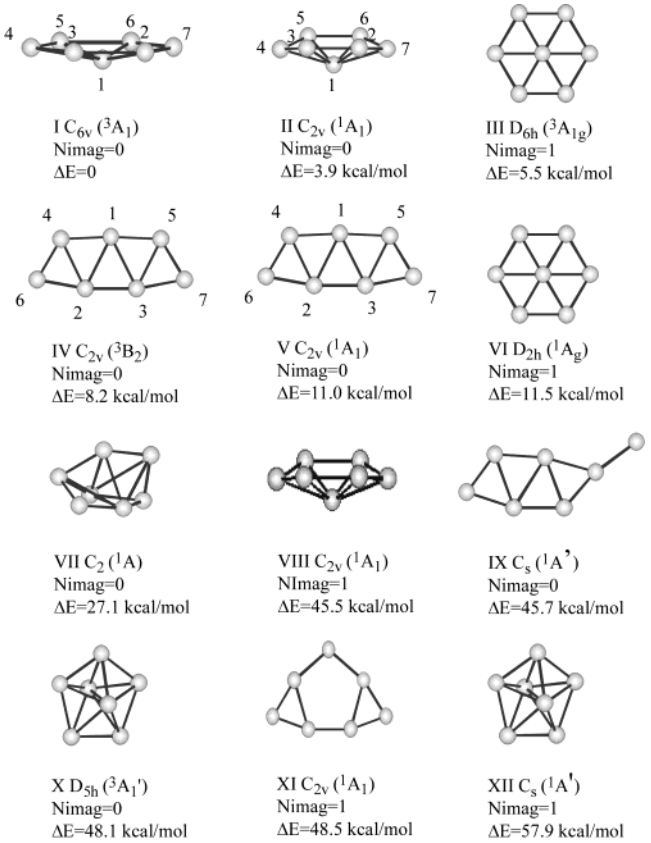

Figure 3. Optimized structures of B_7^- at the B3LYP/6-311+G* level of theory.

TABLE 2: Calculated Molecular Properties of Structure I (Figure 3)—The Global Minimum of B_7^- (C_{6v}, $^3A_1$)[a]

	B3LYP/6-311+G*	RCCSD(T)/6-311+G*
E_{tot}, au	−173.8037621	−173.2344498[b]
R(B1−B2,3,4,5,6,7), Å	1.655	1.683
R(B2−B3), Å	1.606	1.633
$\omega_1(a_1)$, cm^{-1}	917.7 (0.7)	
$\omega_2(a_1)$, cm^{-1}	293.0 (14.3)	
$\omega_3(b_1)$, cm^{-1}	1056.5 (0.0)	
$\omega_4(b_2)$, cm^{-1}	756.2 (0.0)	
$\omega_5(b_2)$, cm^{-1}	352.3 (0.0)	
$\omega_6(e_1)$, cm^{-1}	1120.8 (18.0)	
$\omega_7(e_1)$, cm^{-1}	756.2 (46.0)	
$\omega_8(e_2)$, cm^{-1}	1111.3 (0.0)	
$\omega_9(e_2)$, cm^{-1}	685.4 (0.0)	
$\omega_{10}(e_2)$, cm^{-1}	355.6 (0.0)	

[a] Numbers in parentheses represent infrared intensities. [b] At the RCCSD(T)/6-311+G(2df) level of theory total energy is −173.3156597 au.

that the Hartree−Fock configuration is dominant in all four cases of B_7^- (C_{HF} are 0.953 for the triplet structure I, 0.963 for the singlet structure II, 0.959 for the triplet IV, and 0.832 for the singlet V). Hence, our B3LYP and RCCSD(T) calculations should be reliable.

For the neutral B_7 cluster, the extensive search lead us to the structure XIII (C_{2v}, $^2B_2$) with the electronic configuration $1a_1^2$-$1b_2^2 1b_1^2 2a_1^2 1a_2^2 3a_1^2 2b_1^2 4a_1^2 2b_2^2 3b_1^2 3b_2^1$, as shown in Figure 4 and Table 5. This global minimum structure can be derived from both structures I (C_{6v}, $^3A_1$) and II (C_{2v}, $^1A_1$) of B_7^- by detaching an electron from their HOMOs. No low-lying isomers were found for the neutral B_7 cluster according to our calculations (Figure 4). The planar structure XIV, corresponding to structure IV or V of B_7^-, was 23.1 kcal/mol higher than structure XIII at the B3LYP/6-311+G* level.

TABLE 3: Calculated Molecular Properties of Structure II (Figure 3) of B_7^- (C_{2v}, $^1A_1$)[a]

	B3LYP/6-311+G*	RCCSD(T)/6-311+G*
E_{tot}, au	−173.797532	−173.234794[b]
R (B1−B2,3,5,6)	1.667 Å	1.694 Å
R (B1−B4,7)	1.738 Å	1.781 Å
R (B2−B3)	1.660 Å	1.680 Å
R (B4−B3,5)	1.558 Å	1.590 Å
$\omega_1(a_1)$, cm^{-1}	1129.7 (5.0)	
$\omega_2(a_1)$, cm^{-1}	931.6 (2.4)	
$\omega_3(a_1)$, cm^{-1}	652.2 (0.1)	
$\omega_4(a_1)$, cm^{-1}	440.5 (10.4)	
$\omega_5(a_1)$, cm^{-1}	239.8 (0.8)	
$\omega_6(a_2)$, cm^{-1}	1104.2 (0.0)	
$\omega_7(a_2)$, cm^{-1}	647.7 (0.0)	
$\omega_8(a_2)$, cm^{-1}	422.8 (0.0)	
$\omega_9(b_1)$, cm^{-1}	1183.0 (21.7)	
$\omega_{10}(b_1)$, cm^{-1}	1091.3 (52.6)	
$\omega_{11}(b_1)$, cm^{-1}	694.8 (10.2)	
$\omega_{12}(b_2)$, cm^{-1}	1094.3 (65.5)	
$\omega_{13}(b_2)$, cm^{-1}	796.7 (27.4)	
$\omega_{14}(b_2)$, cm^{-1}	570.3 (2.6)	
$\omega_{15}(b_2)$, cm^{-1}	409.2 (31.6)	

[a] Numbers in parentheses represent infrared intensities. [b] At the RCCSD(T)/6-311+G(2df) level of theory, total energy is −173.314586 au.

6. Interpretation of the Photoelectron Spectra and Comparison with the Theoretical Results

The ab initio calculations suggested that at least two isomers (I and II) could coexist in the B_7^- beam and contribute to the photoelectron spectra of B_7^-. Isomer V could also be present, though it was expected to be weak because it was 7.8 kcal/mol higher than the ground-state structure I at the RCCSD(T)/6-311+G(2df) level of theory. The calculated VDEs from I (into final quartet states only), II, and V at the OVGF level of theory (Table 6) are plotted as vertical bars in Figure 2. The VDEs from IV were also calculated (Table 6) but were not plotted in Figure 2 because it was expected to make negligible contributions to the photoelectron data ($\Delta E = 17.0$ kcal/mol at RCCSD(T)/6-311+G(2df)). Structures I and II gave very similar spectral transitions because they are nearly degenerate and have similar MO pattern. The bottom row is for the lowest energy pyramidal triplet structure I (C_{6v}, $^3A_1$), the middle row is for the lowest energy pyramidal singlet isomer II (C_{2v}, $^1A_1$), and the top row is for the planar singlet isomer V (C_{2v}, $^1A_1$). VDEs with the final doublet states for structure I of B_7^- overlap with the VDEs corresponding to transitions into the similar states for structure II (Table 6). However, the VDEs for structure II are in better agreement (especially at the OVGF/6-311+G(2df) level of theory) with the experimentally observed peaks X, E, F, H, and I. The features A, B, and G could be attributed to contributions from the higher energy planar structure V. Overall, the calculated spectra from the pyramidal and planar structures of B_7^- are in excellent agreement with the experimental data. It seems that the OVGF level of theory works well for the B_7^- system. A more detailed spectral assignment is made in Table 6. The photoelectron spectra of B_7^- were extremely complicated and were not completely resolved because of the spectral congestion. Thus, it is gratifying that the calculated VDEs from the pyramidal and planar structures of B_7^- seem to allow the main spectral features to be well accounted for. In particular, the features A, B, and G were clearly due to the planar isomer V, as the pyramidal structures showed no transitions in these spectral ranges (Figure 2).

It is interesting to note the large energy gaps between the first detachment transition (X) and the second transition (D)

TABLE 4: Calculated Molecular Properties of Structures IV and V (Figure 3) of B_7^- (C_{2v} $^3B_2$ and $^1A_1$)[a]

	IV	V	
method	B3LYP/6-311+G*	B3LYP/6-311+G*	RCCSD(T)/6-311+G*
E_{tot}, au	−173.7906671[b]	−173.7861476	−173.2237467[c]
$R(B_1-B_{2,3})$	1.767 Å	1.999 Å	1.932 Å
$R(B_1-B_{4,5})$	1.596 Å	1.584 Å	1.609 Å
$R(B_1-B_{6,7})$	2.772 Å	2.780 Å	2.814 Å
$\angle(B_2-B_1-B_3)$	54.12°	48.96°	50.98°
$\angle(B_4-B_1-B_5)$	176.68°	162.85°	167.68°
$\angle(B_6-B_1-B_7)$	121.92°	113.82°	116.26°
$\omega_1(a_1)$, cm^{-1}	1366.5 (2.4)	1303.1 (7.5)	
$\omega_2(a_1)$, cm^{-1}	1294.3 (4.6)	1207.4 (0.1)	
$\omega_3(a_1)$, cm^{-1}	787.2 (6.0)	816.9 (10.6)	
$\omega_4(a_1)$, cm^{-1}	617.9 (0.0)	664.7 (2.9)	
$\omega_5(a_1)$, cm^{-1}	467.6 (0.2)	566.4 (4.6)	
$\omega_6(a_1)$, cm^{-1}	399.0 (2.1)	435.1 (0.0)	
$\omega_7(a_2)$, cm^{-1}	456.6 (0.0)	472.2 (0.0)	
$\omega_8(a_2)$, cm^{-1}	91.4 (0.0)	245.7 (0.0)	
$\omega_9(b_1)$, cm^{-1}	368.1 (8.1)	415.9 (1.3)	
$\omega_{10}(b_1)$, cm^{-1}	192.7 (1.0)	183.4 (7.3)	
$\omega_{11}(b_2)$, cm^{-1}	1356.5 (0.4)	1272.6 (3.4)	
$\omega_{12}(b_2)$, cm^{-1}	1154.9 (37.1)	1125.8 (15.3)	
$\omega_{13}(b_2)$, cm^{-1}	1034.8 (3.2)	885.9 (5.8)	
$\omega_{14}(b_2)$, cm^{-1}	530.4 (8.9)	671.3 (1.2)	
$\omega_{15}(b_2)$, cm^{-1}	378.8 (355.1)	534.0 (0.4)	

[a] Numbers in parentheses represent infrared intensities. [b] The total energy E_{tot} at the RCCSD(T)/6-311+G* level of theory is −173.2145336 au and at the RCCSD(T)/6-311+G(2df) level of theory is −173.288645 au. [c] The total energy E_{tot} at the RCCSD(T)/6-311+G(2df) level of theory is −173.3033020 au.

TABLE 5: Calculated Molecular Properties of B_7 (C_{2v}, $^2B_2$) Global Minimum Structure XIII (Figure 4)[a]

	B3LYP/6-311+G*	RCCSD(T)/6-311+G*
E_{tot}, au	−173.7102201	−173.1415275[b]
R(B1−B2,3,5,6)	1.691 Å	1.718 Å
R(B1−B4,7)	1.764 Å	1.757 Å
R(B2−B3)	1.622 Å	1.646 Å
R(B4−B3,5)	1.557 Å	1.595 Å
$\omega_1(a_1)$, cm^{-1}	1181.4 (1.1)	
$\omega_2(a_1)$, cm^{-1}	925.4 (3.5)	
$\omega_3(a_1)$, cm^{-1}	612.9 (0.1)	
$\omega_4(a_1)$, cm^{-1}	449.6 (4.5)	
$\omega_5(a_1)$, cm^{-1}	273.8 (0.1)	
$\omega_6(a_2)$, cm^{-1}	1101.3 (0.0)	
$\omega_7(a_2)$, cm^{-1}	599.4 (0.0)	
$\omega_8(a_2)$, cm^{-1}	358.0 (0.0)	
$\omega_9(b_1)$, cm^{-1}	1217.7 (12.4)	
$\omega_{10}(b_1)$, cm^{-1}	1062.5 (167.7)	
$\omega_{11}(b_1)$, cm^{-1}	763.7 (14.6)	
$\omega_{12}(b_2)$, cm^{-1}	1028.7 (66.9)	
$\omega_{13}(b_2)$, cm^{-1}	793.0 (66.9)	
$\omega_{14}(b_2)$, cm^{-1}	617.4 (2.1)	
$\omega_{15}(b_2)$, cm^{-1}	416.0 (16.3)	

[a] Numbers in parentheses represent infrared intensities. [b] At the RCCSD(T)/6-311+G(2df) level of theory, total energy is −173.2111598 au.

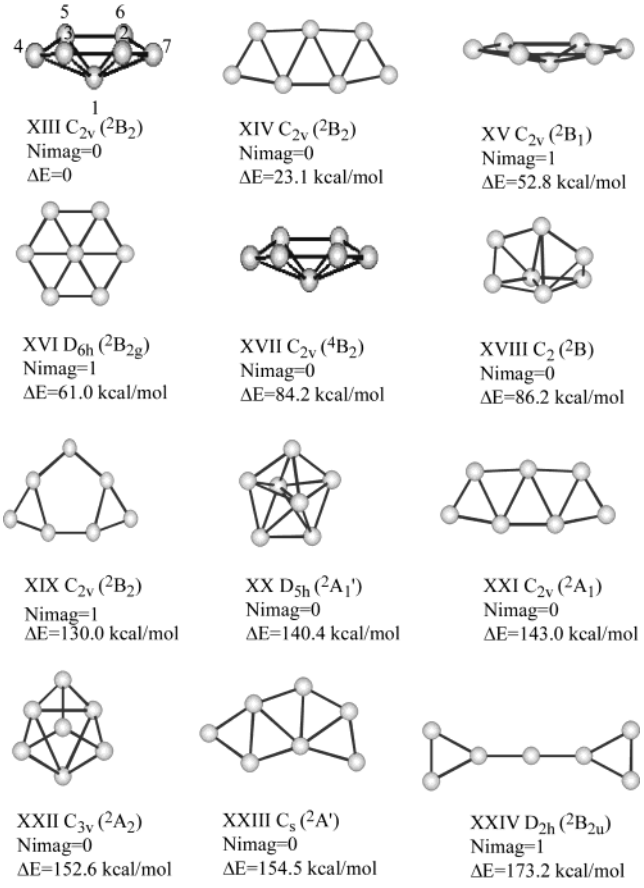

Figure 4. Optimized structures of B_7 at the B3LYP/6-311+G* level of theory.

for both of the pyramidal isomers (Table 6). This large energy gap suggested that the two electrons in the HOMO of these two isomers are relatively unstable and their removal would produce a much more electronically stable B_7^+. This expectation was supported by previous experimental studies, which did show that B_7^+ was an extremely stable cation.[35] This observation provided another confirmation for the validity of the interpretation of the B_7^- photoelectron spectra.

Thus, the feature A represents the transition from the ground state of the planar structure (V) to the ground state of the neutral planar structure (XIV). The A band was very sharp with a short vibrational progression, suggesting very small geometrical changes from the anion to the neutral. This observation was born out from the calculated structures. On the other hand, the X band, which represents the transitions from the pyramidal B_7^- (I) to the neutral pyramidal B_7 (XIII), was very broad, consistent with the large geometry changes between structures I and XIII. The relatively high VDEs of the planar isomers were due to the fact that the planar structure was much more unstable

TABLE 6: Calculated VDEs of B_7^- at Different Levels of Theory for Structures I, II, IV, and V, and Recommended PES Data Assignments[g]

		theoretical VDE[a]				PES data assignment	
isomer	calculated transition	U(R)OVGF/ 6-311+G(2 df)	RCCSD(T)/ 6-311+G(2df)	TD-B3LYP/ 6-311+G(2df)	TD-BPW916-311+G(2df)	obsd feature	exp VDE
I (C_{6v},$^3A_1$)[c]	$3e_1\,\alpha \rightarrow {}^2E_1$	2.74 (0.91)	2.89	2.80	2.95	X	2.85
	$2e_1\,\beta \rightarrow {}^4E_1$	4.02 (0.89)	4.14	3.96	3.88	D	4.05
	$2e_1\,\alpha \rightarrow {}^2E_1$	[4.28 (0.90)][b]		4.04	3.93		
	$3a_1\,\beta \rightarrow {}^4A_1$	5.27 (0.91)	5.85	5.35	5.13	H	5.32
	$1b_1\,\beta \rightarrow {}^4B_1$	5.60 (0.90)	5.96	5.39	5.36	I	5.64
	$1b_1\,\alpha \rightarrow {}^2B_1$	[5.61 (0.90)][b]		4.71	4.72		
	$3a_1\,\beta \rightarrow {}^2A_1$	[6.35 (0.84)][b]		5.18	5.04		
	$2a_1\,\beta \rightarrow {}^2A_1$	[7.00 (0.80)][b]		5.36	5.05		
II (C_{2v},$^1A_1$)[d]	$3b_2 \rightarrow {}^2B_2$	2.70 (0.88)	2.83	2.59	2.65	X	2.85
	$3b_1 \rightarrow {}^2B_1$	4.07 (0.87)	4.20	4.18	4.07	E	4.21
	$2b_2 \rightarrow {}^2B_2$	4.29 (0.88)		4.33	4.30	F	4.35
	$2b_1 \rightarrow {}^2B_1$	5.31 (0.87)		5.32	5.08	H	5.32
	$4a_1 \rightarrow {}^2A_1$	5.66 (0.80)	5.87	5.93	5.89	I	5.64
IV (C_{2v},$^3B_2$)[e]	$6a_1 \rightarrow {}^2B_2$	3.54 (0.90)	3.09	3.39	3.27		
	$1a_2 \rightarrow {}^4B_1$	3.28 (0.90)	3.60	3.49	3.51		
	$4b_2 \rightarrow {}^2A_1$	3.62 (0.89)	4.12	4.26	4.23		
	$5a_1 \rightarrow {}^4B_2$	4.44 (0.89)	4.73	4.48	4.46		
	$4a_1 \rightarrow {}^4B_2$	4.27 (0.90)		4.61	4.54		
	$3b_2 \rightarrow {}^4A_1$	5.42 (0.85)	5.36	5.18	5.05		
	$1b_1 \rightarrow {}^4A_2$	5.84 (0.84)	5.78	5.99	5.81		
V (C_{2v},$^1A_1$)[f]	$4b_2 \rightarrow {}^2B_2$	3.40 (0.86)	3.51	3.10	3.06	A	3.44
	$1a_2 \rightarrow {}^2A_2$	3.67 (0.88)	3.69	3.55	3.68	B	3.71
	$5a_1 \rightarrow {}^2A_1$	4.92 (0.83)	4.81	4.72	4.52	G	4.60
	$4a_1 \rightarrow {}^2A_1$	4.97 (0.83)		5.33	5.27		
	$1b_1 \rightarrow {}^2B_1$	5.69 (0.83)	5.78	5.84	5.76		
	$3b_2 \rightarrow {}^2B_2$	5.80 (0.84)		5.49	5.35		

[a] The numbers in parentheses indicate the pole strength, which characterizes the validity of the one-electron detachment picture. [b] Vertical electron detachment energies calculated at the UOVGF level of theory leading to the final doublet states should be considered as very crude because of the multiconfigurational nature of the reference wave function in the final doublet states. [c] At the RCCSD(T)/6-311+G(2df) level of theory, $\Delta E = 0.0$ kcal/mol. [d] At the RCCSD(T)/6-311+G(2df) level of theory, $\Delta E = 0.7$ kcal/mol. [e] At the RCCSD(T)/6-311+G(2df) level of theory, $\Delta E = 17.0$ kcal/mol. [f] At the RCCSD(T)/6-311+G(2df) level of theory, $\Delta E = 7.8$ kcal/mol. [g] All energies are in eV.

in the neutrals than in the anions, which was born out from the theoretical calculations (Figure 4).

Our photoelectron spectra showed that the planar isomer V of B_7^-, even though significantly less favorable energetically than the pyramidal ones, was quite abundant. Its spectral intensities were as intense as the more stable pyramidal B_7^-. This was rather surprising because the planar isomer V was not expected to be so abundant on the basis of the energetics. This was one of the factors contributing to our initial confusions about the B_7^- photoelectron spectra. The high abundance of the planar B_7^- isomer must be due to its high kinetic stability and can be understood from the cluster growth mechanisms. Our previous studies showed that all smaller B_n^- clusters have perfect 2D structures. Both B_6^- and B_6 have two low-lying planar structures, one D_{2h} and one C_{2h}. Addition of one B atom to any of these structures would lead to the planar B_7^- structure with small structural changes. On the other hand, formation of the pyramidal B_7^- from the D_{2h} or C_{2h} hexamer by addition of one B atom would involve significant structural rearrangement.

7. Chemical Bonding in the Pyramidal and Planar B_7^-

7.1. Chemical Bonding in the Triplet Pyramidal C_{6v} B_7^- Structure: π and σ Aromaticity and Comparison to That in B_8. To understand the chemical bonding in the lowest energy pyramidal B_7^-, we performed a detailed molecular orbital analysis. The molecular orbitals of the triplet structure I (C_{6v}, $^3A_1$) and corresponding planar isomer III (D_{6h}, $^3A_{1g}$) for B_7^- are presented in Figure 5A and B. Even though structure I is not perfectly planar, we may approximately use the σ and π designations to the molecular orbitals, because the deviation from planarity is rather small and the barrier of planarization is small, too. Out of the 12 valence molecular orbitals, the HOMO and HOMO′ ($3e_1$) and HOMO-4 ($2a_1$) are a set of π orbitals (which can be more clearly seen in Figure 5B for the planar structure III) and give the triplet C_{6v} structure π-aromaticity. Even though there are only four π electrons, it was shown that for triplet states the reversed Huckel rule, that is, $4n$ instead of $(4n + 2)$, should be obeyed for aromaticity.

The HOMO-1, HOMO-1′, and HOMO-2 in structure I (C_{6v}, $^3A_1$) represent a set of σ orbitals largely responsible for the radial bonding between the apex atom and the six peripheral atoms. Again, HOMO-1 and HOMO-1′ in Figure 5B demonstrate that more clearly in the planar structure III. The three σ orbitals cannot be localized to three classical 2c−2e bonds and have to be shared by the six radial bonds, giving characteristics of σ-aromaticity. Thus, the triplet structure I (C_{6v}, $^3A_1$) of B_7^- can be considered as being doubly (σ and π) aromatic, as it was previously found for B_8, B_8^{2-}, and B_9^-.[45] These six valence molecular orbitals are mainly responsible for the chemical bonding between the central atom and the peripheral atoms. The other six valence molecular orbitals (HOMO-3, HOMO-5, HOMO-5′, HOMO-6, HOMO-6′, and HOMO-7) are responsible for peripheral bonding between boron atoms forming the hexagonal ring. To show this more clearly, we optimized a model cyclic structure of Be_6 (D_{6h}, $^1A_{1g}$), which has six occupied molecular orbitals (Figure 6) similar to the set in Figure 5 identified to be responsible for the bonding within the hexagonal ring. We could localize the six valence molecular orbitals of Be_6 into six 2e−2c sp_σ−sp_σ Be−Be bonds using the natural bond analysis, proving that indeed these molecular orbitals are responsible for the peripheral bonding in the Be_6 and B_6 (in B_7^- and B_7) rings. The highly symmetrical structure I (C_{6v}, $^3A_1$)

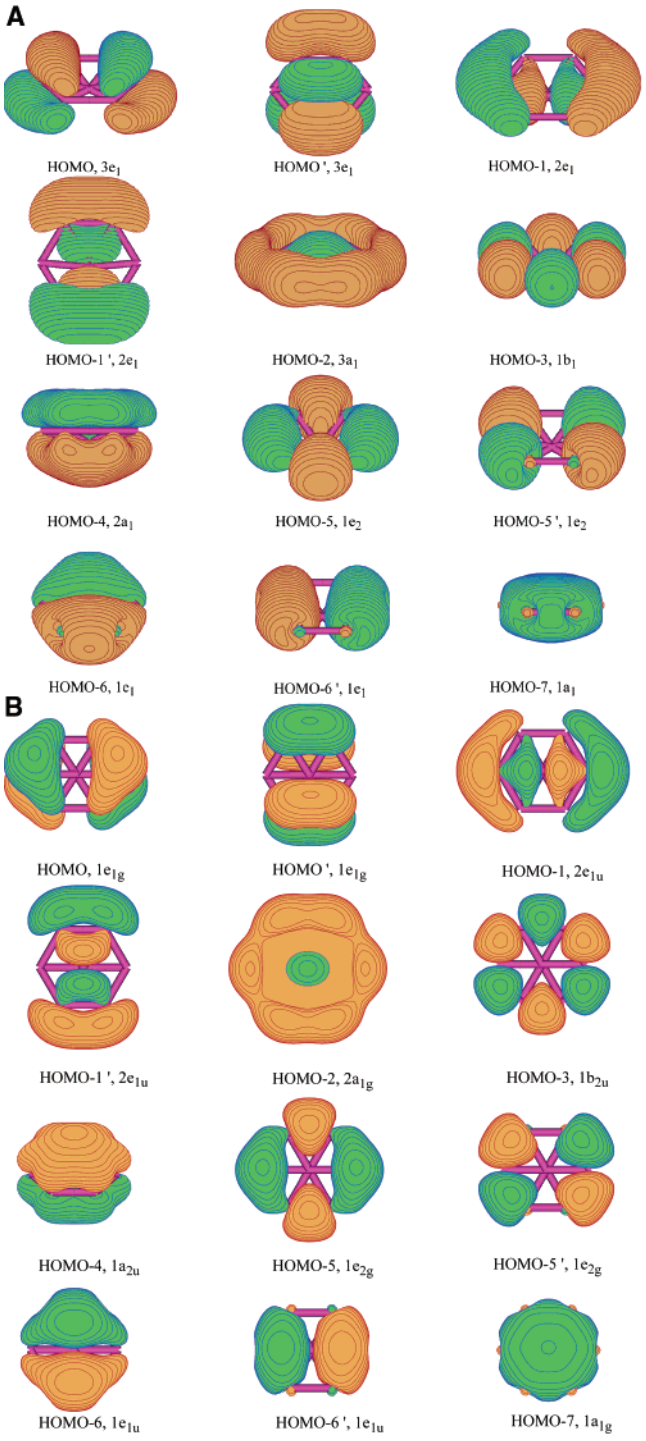

Figure 5. (A) Molecular orbital pictures for the global minimum structure I (C_{6v}, $^3A_1$) of B_7^-. The order of MOs is according to the OVGF calculation. (B) Molecular orbital pictures for the structure III (D_{6h}, $^3A_{1g}$) of B_7^-.

of B_7^- is consistent with the presence of double aromaticity. The slight nonplanarity is a result of the small size of the central cavity formed by the B_6 ring. A B_7 ring has the right size, giving the perfect D_{7h} planar structure for B_8.[45]

7.2 The Chemical Bonding in the Singlet Pyramidal C_{2v} and Planar D_{2h} B_7^- Structures: π-Antiaromaticity and σ-Aromaticity. Molecular orbitals for the C_{2v} ($^1A_1$) structure II and corresponding planar isomer VI (D_{2h}, ^1A_g) are shown in Figure 7A and B. One can see that their molecular orbitals are similar to those of the C_{6v} ($^3A_1$) structure I (Figure 5A), except that in singlet structures only one orbital of the pair of the doubly

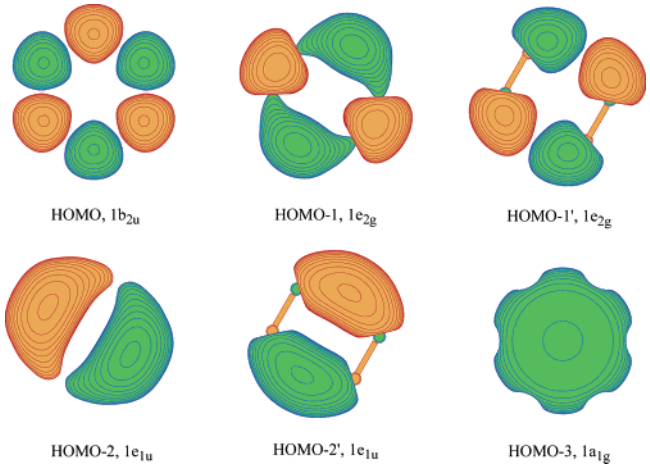

Figure 6. Molecular orbital pictures for the model cyclic structure of Be_6 (D_{6h}, $^1A_{1g}$).

degenerate HOMO ($3e_1$) is occupied. To make a relation between molecular orbital occupation and geometric structure, let us first consider distortion in the plane. An occupation of the doubly degenerate HOMO ($1e_{1g}$) by a singlet pair of electrons results in a Jahn−Teller distortion from the D_{6h} ($^3A_{1g}$) structure III toward D_{2h} (^1A_g) structure VI when planarity is preserved. However, structure VI is not a minimum and optimization following the imaginary frequency leads to structure II. The direction of the distortion can be understood on the basis of the bonding pattern in the HOMO of structures VI, III, and II. The $3b_2$-MO and $3a_1$-MO in structure II can be approximately considered as π-MO and thus the regular $4n$ Hückel rule for antiaromatic systems is obeyed. The π-character of $3b_2$-MO and $3a_1$-MO in structure II can be clearly seen in that we correlate these MOs to the corresponding $1b_{2g}$-MO and $2b_{1u}$-MO in the D_{2h} ($^1A_{1g}$) isomer VI. The σ molecular orbitals in both the C_{2v} ($^1A_1$) and the D_{2h} ($^1A_{1g}$) (HOMO-1, HOMO-2, HOMO-3, Figure 7A and B) and the C_{6v} ($^3A_1$) (HOMO-1, HOMO-1′, HOMO-2) structures are similar; thus all three isomers have similar σ-aromaticity. This gives the C_{2v} ($^1A_1$) structure II and the D_{2h} ($^1A_{1g}$) structure VI the unusual characters of being π-antiaromatic and σ-aromatic.

7.3. The Chemical Bonding in the Singlet Planar C_{2v} B_7^- Structure: σ- and π Antiaromaticity. The molecular orbitals of the singlet C_{2v} planar structure V is shown in Figure 8. This isomer possesses two π-orbitals (HOMO-1 and HOMO-4) and nine σ valence orbitals. The σ orbitals describing the in-plane B−B bonding are highly delocalized. In the D_{7h} structure of B_7^-, we should expect that seven σ-orbitals are responsible for the peripheral B−B bonding similar as it was discussed above for the D_{6h} Be_6 and B_6 structures. Thus, we have only two σ-orbitals for bonding through the center in the D_{7h} cluster. Two occupied π-orbitals in the D_{7h} structure of B_7^- render the π-antiaromaticity and two occupied σ-orbitals responsible for bonding through the center of the cluster render the σ-antiaromaticity. The double antiaromaticity leads to the distortion of the D_{7h} structure into the C_{2v} planar structure V. The elongated shape of this isomer is consistent with the structural distortions imposed by antiaromaticity. This is similar to the ground state of B_6^{2-} (D_{2h}), which also possesses four π electrons and is antiaromatic.[44,29] Recently, we have found that larger boron clusters also follow the $4n$ Hückel rule for antiaromaticity.[46] For example, both B_{13}^- and B_{14} each with eight π electrons are antiaromatic and also possess elongated ground-state structures because of antiaromaticity.[46] Thus, we have shown

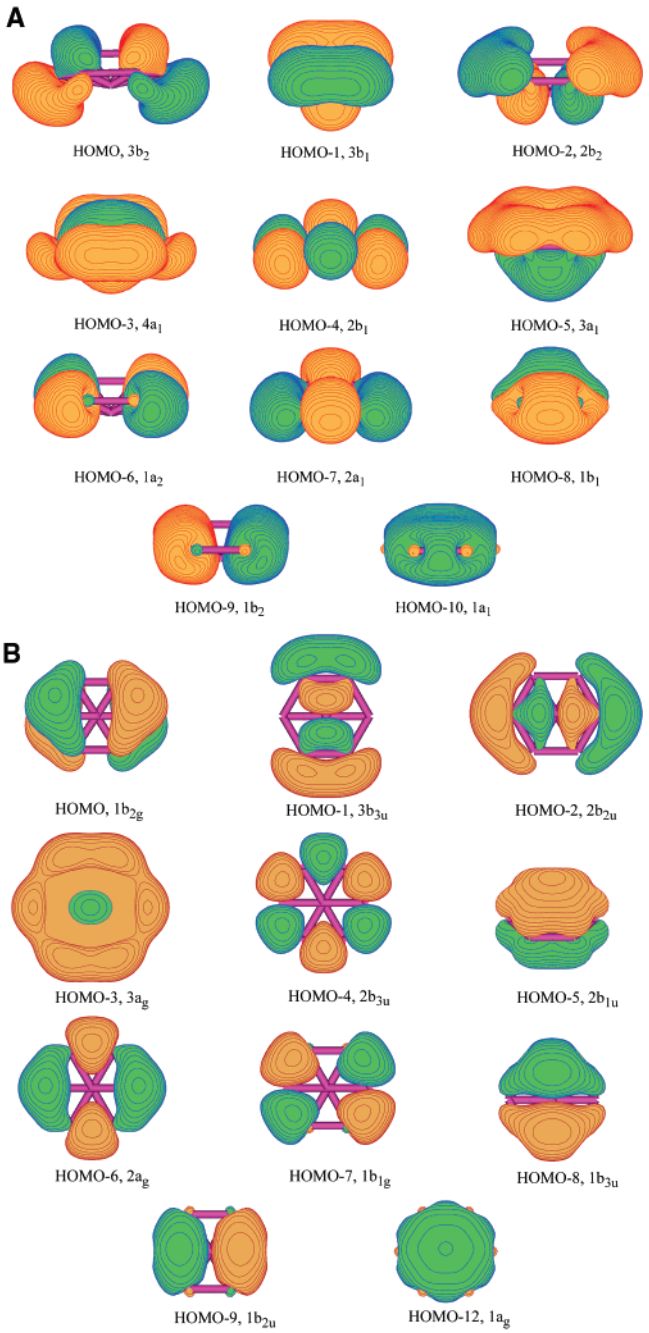

Figure 7. (A) Molecular orbital pictures for structure II (C_{2v}, $^1A_1$) of B_7^-. The order of MOs is according to the OVGF calculation. (B) Molecular orbital pictures for structure VI (D_{2h}, ^1A_g) of B_7^-.

that aromaticity and antiaromaticity are unique characteristics of the planar boron clusters.

8. Conclusions

We report a combined experimental and theoretical investigation of the structure and bonding of B_7^-. Complicated and well-resolved photoelectron spectra were obtained for the anionic B_7^- species at various photon energies and direct experimental evidence was presented for the coexistence of different B_7^- isomers. An extensive search for the global minimum was performed for B_7^- and B_7 at the B3LYP/6-311+G* level of theory. Two pyramidal structures of B_7^- were the most stable: a triplet C_{6v} and a singlet C_{2v} structure. A third isomer, a perfectly planar singlet structure V (C_{2v}, $^1A_1$), was 7.8 kcal/mol higher (RCCSD(T)/6-311+G(2df) and was a major contributor to the observed B_7^- photoelectron spectra. The complicated photoelectron patterns can be well interpreted when all the three lowest energy structures were included. Molecular orbital analyses for the B_7^- systems revealed a double-aromatic character (π and σ) for the triplet pyramidal C_{6v} structure (I), σ-aromatic and π-antiaromatic character for the singlet pyramidal C_{2v} structure (II), and 5- and π-antiaromatic character for the singlet planar C_{2v} structure (V). Thus, the last member of the B_3-B_{15} series of clusters has been now characterized experimentally and theoretically. We found along this series that aromaticity and antiaromaticity play an important role in the chemical bonding, structure, and stability of the small boron clusters.[42−46]

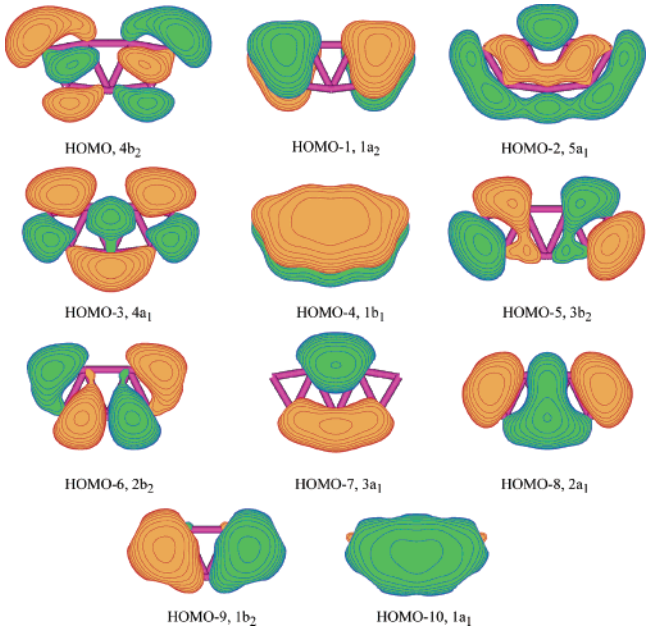

Figure 8. Molecular orbital pictures for structure V (C_{2v}, $^1A_1$) of B_7^-. The order of MOs is according to the OVGF calculation.

Acknowledgment. The theoretical work done at Utah was supported by the donors of the Petroleum Research Fund (ACS-PRF# 38242-AC6), administered by the American Chemical Society. The experimental work done at Washington was supported by the National Science Foundation (DMR-0095828) and performed at the W. R. Wiley Environmental Molecular Sciences Laboratory, a national scientific user facility sponsored by DOE's Office of Biological and Environmental Research and located at Pacific Northwest National Laboratory, which is operated for DOE by Battelle.

References and Notes

(1) Cotton, F. A.; Wilkinson, G.; Murillo, C. A.; Bochmann, M. *Advanced Inorganic Chemistry*, 6th ed.; John Wiley & Sons: New York, 1999.
(2) Greenwood, N. N.; Earnshaw, A. *Chemistry of Elements*, 2nd ed.; Buttwerworth-Heinemann: Oxford, U.K., 1997.
(3) Tang, A. C.; Li, Q. S. *Int. J. Quantum Chem.* **1986**, *29*, 579.
(4) Hanley, L.; Whitten, J. L.; Anderson S. L. *J. Phys. Chem.* **1988**, *92*, 5803.
(5) Hernandez, R.; Simons, J. *J. Chem. Phys.* **1991**, *94*, 2961.
(6) Kato, A. U.; Tanaka E. *J. Comput. Chem.* **1991**, *12*, 1097.
(7) Kato, A. U.; Yamashita, K.; Morokuma, K. *Chem. Phys. Lett.* **1992**, *190*, 361.
(8) Martin, J. M. L.; Francois, J. P.; Gijbels, R. *Chem. Phys. Lett.* **1992**, *189*, 529.
(9) Kawai, R.; Weare, J. H. *Chem. Phys. Lett.* **1992**, *191*, 311.
(10) Ray, A. K.; Howard, I. A.; Kanal, K. M. *Phys. Rev. B* **1992**, *45*, 14247.
(11) Boustani, I. *Int. J. Quantum Chem.* **1994**, *52*, 1081.

(12) Meden, A.; Mavri, J.; Bele, M.; Pejovnik, S. *J. Phys. Chem.* **1995**, *99*, 4252.
(13) Boustani, I. *Chem. Phys. Lett.* **1995**, *233*, 273.
(14) Boustani, I. *Chem. Phys. Lett.* **1995**, *240*, 135.
(15) Boustani, I. *Surf. Sci.* **1996**, *370*, 355.
(16) Ricca, A.; Bauschlicher, C. W. *Chem. Phys*. **1996**, *208*, 233.
(17) Ricca, A.; Bauschlicher, C. W. *J. Chem. Phys.* **1997**, *106*, 2317.
(18) Niu, J.; Rao, B. K.; Jena, P. *J. Chem. Phys.* **1997**, *107*, 132.
(19) Boustani, I. *Phys. Rev. B* **1997**, *55*, 16426.
(20) Gu, F. L.; Yang, X. M.; Tang, A. C.; Jiao, H. J.; Schleyer, P. v. R. *J. Comput. Chem.* **1998**, *19*, 203.
(21) Boustani, I.; Quandt, A. *Comput. Mater. Sci.* **1998**, *11*, 132.
(22) Boustani, I.; Rubio, A.; Alonso, J. A. *Chem. Phys. Lett*. **1999**, *311*, 21.
(23) McKee, M. L.; Wang, Z. X.; Schleyer, P. v. R. *J. Am. Chem. Soc*. **2000**, *122*, 4781.
(24) Fowler, J. E.; Ugalde, J. M. *J. Phys. Chem. A* **2000**, *104*, 397.
(25) Aihara, J. *J. Phys. Chem. A* **2001**, *105*, 5486.
(26) Cao, P.; Zhao, W.; Li, B.; Song, B.; Zhou, X. *J. Phys.: Condens. Matter* **2001**, *13*, 5065.
(27) Petters, A.; Alsenoy, C. V.; March, N. H.; Klein, D. J.; Van Doren, V. E. *J. Phys. Chem. B* **2001**, *105*, 10546.
(28) Luo, W.; Clancy, P. *J. Appl. Phys.* **2001**, *89*, 1596.
(29) Havenith, R. W. A.; Fowler, P. W.; Steiner, E. *Chem. Eur. J.* **2002**, *8*, 1068.
(30) Li, Q. S.; Jin, H. W. *J. Phys. Chem. A* **2002**, *106*, 7042.
(31) Ma, J.; Li, ZH.; Fan, KN.; Zhou, M. F. *Chem. Phys. Lett.* **2002**, *372*, 708.
(32) Jin, H. W.; Li, Q. S. *Phys. Chem. Chem. Phys*. **2003**, *5*, 1110.
(33) Li, Q. S.; Jin, Q.; Luo, Q.; Tang, A. C.; Yu, J. K.; Zhang, H. X. *Int. J. Quantum Chem.* **2003**, *94*, 269.
(34) Li, Q. S.; Jin, Q. *J. Phys. Chem. A* **2003**, *107*, 7869.
(35) Hanley, L.; Anderson, S. L. *J. Phys. Chem.* **1987**, *91*, 5161. Hanley, L.; Whitten, J. L.; Anderson, S. L. *J. Phys. Chem*. **1988**, *92*, 5803.
(36) Hanley, L.; Anderson, S. L. *J. Chem. Phys.* **1988**, *89*, 2848.
(37) Hintz, P. A.; Ruatta, S. A.; Anderson, S. L. *J. Chem. Phys.* **1990**, *92*, 292.
(38) Ruatta, S. A.; Hintz, P. A.; Anderson, S. L. *J. Chem. Phys.* **1991**, *94*, 2833.
(39) Hintz, P. A.; Sowa, M. B.; Ruatta, S. A.; Anderson, S. L. *J. Chem. Phys.* **1991**, *94*, 6446.
(40) Placa, S. J. La; Roland, P. A.; Wynne, J. J. *Chem. Phys. Lett.* **1992**, *190*, 163.
(41) Sowa-Resat, M. B.; Smolanoff, J.; Lapiki, A.; Anderson, S. L. *J. Chem. Phys.* **1997**, *106*, 9511.
(42) Zhai, H.-J.; Wang, L.-S.; Alexandrova, A. N.; Boldyrev, A. I.; Zakrzewski. V. G. *J. Phys. Chem. A* **2003**, *107*, 9319.
(43) Zhai, H.-J.; Wang, L.-S.; Alexandrova, A. N.; Boldyrev, A. I. *J. Chem. Phys*. **2002**, *117*, 7917.
(44) Alexandrova, A. N.; Boldyrev, A. I.; Zhai, H.-J.; Wang, L.-S.; Sheiner, E.; Fowler, P. W. *J. Phys. Chem. A* **2003**, *107*, 1359.
(45) Zhai, H.-J.; Wang, L.-S.; Alexandrova, A. N.; Boldyrev. A. I. *Angew. Chem., Int. Ed.* **2003**, *42*, 6004.
(46) Zhai, H.-J.; Kiran, B.; Li, J.; Wang, L.-S. *Nature Mater.* **2003**, *2*, 827.
(47) Wang, L. S.; Cheng, H. S.; Fan, J. *J. Chem. Phys.* **1995**, *102*, 9480. Wang, L. S.; Wu, H. In *Advances in Metal and Semiconductor Clusters. IV. Cluster Materials*; Duncan, M. A., Ed.; JAI Press: Greenwich, CT, 1998; p 299.
(48) Xu, S. J.; Nilles, J. M.; Radisic, D.; Zheng, W. Z.; Stokes, S.; Bowen, K. H.; Becker, R. C.; Boustani, I. *Chem. Phys. Lett*. **2003**, *379*, 282.
(49) Parr R. G.; Yang W. *Density-functional theory of atoms and molecules*; Oxford University Press: Oxford, UK, 1989.
(50) Becke A. D. *J. Chem. Phys.* **1993**, *98*, 5648.
(51) Perdew J. P.; Chevary J. A.; Vosko S. H.; Jackson K. A.; Pederson M. R.; Singh D. J.; Fiolhais C. *Phys. Rev. B* **1992**, *46*, 6671.
(52) McLean A. D.; Chandler G. S. *J. Chem. Phys.* **1980**, *72*, 5639.
(53) Clark T.; Chandrasekhar J.; Spitznagel G. W.; Schleyer P. v. R. *J. Comput. Chem*. **1983**, *4*, 294.
(54) Frisch M. J.; Pople J. A.; Binkley J. S. *J. Chem. Phys.* **1984**, *80*, 3265.
(55) Cizek, J. *Adv. Chem. Phys.* **1969**, *14*, 35.
(56) Knowles, P. J.; Hampel, C.; Werner, H.-J. *J. Chem. Phys.* **1993**, *99*, 5219.
(57) Raghavachari, K.; Trucks, G. W.; Pople, J. A.; Hrad-Gordon, M. *Chem. Phys. Lett.* **1989**, *157*, 479.
(58) Bernardi, F.; Bottini, A.; McDougall, J. J. W.; Robb, M. A.; Schlegel, H. B. *Faraday Symp. Chem. Soc*. **1979**, *19*, 137.
(59) Frisch, M. J.; Ragazos, I. N.; Robb, M. A.; Schlegel, H. B. *Chem. Phys. Lett*. **1992**, *189*, 524.
(60) Cederbaum L. S. *J. Phys B* **1975**, *8*, 290.
(61) von Niessen, W.; Shirmer, J.; Cederbaum, L. S. *Comput. Phys. Rep.* **1984**, *1*, 57.
(62) Zakrzewski, V. G.; von Niessen, W. *J. Comput. Chem.* **1993**, *14*, 13.
(63) Stratmann, R. E.; Scuseria, G. E.; Frisch, M. J. *J. Chem. Phys.* **1998**, *109*, 8218.
(64) (a) Ortiz, J. V. *Int. J. Quantum Chem., Quantum Chem. Symp*. **1989**, *23*, 321. (b) Lin, J. S.; Ortiz, J. V. *Chem. Phys. Lett*. **1990**, *171*, 197.
(65) Zakrzewski, V. G.; Ortiz, J. V.; Nichols, J. A.; Heryadi, D.; Yeager, D. L.; Golab, J. T. *Int. J. Quantum Chem., Quant*. **1996**, *60*, 29.
(66) Bauernshmitt, R.; Alrichs, R. *Chem. Phys. Lett.* **1996**, *256*, 454.
(67) Casida, M. E.; Jamorski, C.; Casida, K. C.; Salahub, D. R. *J. Chem. Phys*. **1998**, *108*, 4439.
(68) Frisch, M. J.; Trucks, G. M.; Schlegel, H. B.; Scuseria, G. E.; Robb, M. A.; Cheeseman, J. R.; Zakrzewski, V. G.; Montgomery, J. A.; Stratmann, R. E. Jr.; Burant, J. C.; Dapprich, S.; Millam, J. M.; Daniels, A. D.; Kudin, K. N.; Strain, M. C.; Farkas, O.; Tomasi, J.; Barone, V.; Cossi, M.; Cammi, R.; Mennucci, B.; Pomelli, C.; Adamo, C.; Clifford, S.; Ochterski, J. W.; Petersson, G.A.; Ayala, P. Y.; Cui, Q.; Morokuma, K.; Salvador, P.; Dannenberg, J. J.; Malick, D. K.; Rabuck, A. D.; Raghavachari, K.; Foresman, J. B.; Cioslowski, J.; Ortiz, J. V.; Baboul, A. G.; Stafanov, B. B.; Liu, G.; Liashenko, A.; Piskorz, P.; Komaromi, I.; Gomperts, R.; Martin, R. L.; Fox, D. J.; Keith, T.; Al-Laham, M. A.; Peng, C. Y.; Nanayakkara, A.; Challacombe, M.; Gill, P. M. W.; Johnson, B. G.; Chen, W.; Wong, M. W.; Andres, J. L.; Head-Gordon, M.; Replogle, E. S.; Gonzales, C.; Pople, J. A. *Gaussian 98 (revision A.7)* Gaussian Inc.: Pittsburgh, PA, 1998.
(69) Frisch, M. J.; Trucks, G. M.; Schlegel, H. B.; Scuseria, G. E.; Robb, M. A.; Cheeseman, J. R.; Montgomery, J. A.; Vreven, T.; Kudin, K. N.; Burant, J. C.; Millam, J. M.; Iyengar, S. S.; Tomasi, J.; Barone, V.; Mennucci, B.; Cossi, M.; Scalmani, G.; Rega, N.; Petersson, G. A.; Nakatsuji, H.; Kitao, O.; Nakai, H.; Klene, M.; Li, X.; Knox, J. E.; Hratchian, H. P.; Cross, J. B.; Adamo, C.; Jaramillo, J.; Gomperts, R.; Stratmann, R. E.; Yazyev, O.; Austin, A. J.; Cammi, R.; Pomelli, C.; Ochterski, J. W.; Ayala, P. Y.; Morokuma, K.; Voth, G. A.; Salvador, P.; Dannenberg, J. J.; Zakrzewski, V. G.; Dapprich, S.; Daniels, A. D.; Strain, M. C.; Farkas, O.; Malick, D. K.; Rabuck, A. D.; Raghavachari, K.; Foresman, J. B.; Ortiz, J. V.; Cui, Q.; Baboul, A. G.; Clifford, S.; Cioslowski, J.; Stefanov, B. B.; Liu, G.; Liashenko, A.; Piskorz, P.; Komaromi, I.; Martin, R. L.; Fox, D. J.; Keith, T.; Al-Laham, M. A.; Peng, C. Y.; Nanayakkara, A.; Challacombe, M.; Gill, P. M. W.; Johnson, B. G.; Chen, W.; Wang, M. W.; Gonzales, C.; Pople, J. A. *Guassian 03 (revision A.1)* Gaussian Inc.: Pittsburgh, PA, 2003.
(70) MOLPRO-2000.1. H.-J. Werner, P. J. Knowles, with contributions from R. D. Amos, A. Bernhardsson, A. Berning, P. Celani, D. L. Cooper, M. J. O. Deegan, A. J. Dobbyn, F. Eckert, C. Hampel, G. Hetzer, T. Korona, R. Lindh, A. W. Llpyd, S. J. McNicholas, F. R. Manby, W. Meyer, M. E. Mura, A. Nicklass, P. Palmieri, R. Pitzer, G. Rauhut, M. Schutz, H. Stoll, A. J. Stone, R. Tarroni, and T. Thorsteinsson. Birmingham, UK, 1999.
(71) Schaftenaar, G. *MOLDEN3.4*; MOLDEN3.4, CAOS/CAMM Center: The Netherlands, 1998.
(72) Wang, L. S.; Li, X. Temperature effects in anion photoelectron spectroscopy of metal clusters. In *Clusters and Nanostructure Interfaces*; Jena, P., Khanna, S. N., Rao, B. K., Eds.; World Scientific: Singapore, 2000; pp 293−300.